Fuel 341 (2023) 127690

Contents lists available at ScienceDirect

Fuel

journal homepage: www.elsevier.com/locate/fuel

Full Length Article

CO_2-SR technology using NiBa unsupported catalyst. Isotopic study of cyclic process of CO_2 storage and *in situ* regeneration with CH_4

S. Molina-Ramírez [a], D. Peltzer [b], M. Cortés-Reyes [a], C. Herrera [a], M.A. Larrubia [a], L. Cornaglia [b], L.J. Alemany [a,*]

[a] Departamento de Ingeniería Química, Facultad de Ciencias, Campus de Teatinos, Universidad de Málaga, Málaga E-29071, Spain
[b] Instituto de Investigaciones en Catálisis y Petroquímica (INCAPE), Universidad Nacional del Litoral, CONICET, Facultad de Ingeniería Química, Santiago del Estero, 2829-3000 Santa Fe, Argentina

ARTICLE INFO

Keywords:
CO_2 storage and regeneration
NiBa unsupported catalyst
Isotopic study
Reaction pathways
Syngas production

ABSTRACT

The unsupported NiBa catalyst has been used in the CO_2-SR (CO_2 Storage and in situ Regeneration with CH_4) cyclic technology, which allows the use of CO_2 from combustion and CH_4 from biogas in order to produce enriched syngas streams. The isotopic study in transient regime, using $^{13}CO_2$ and CD_4 instead of $^{12}CO_2$ and CH_4, respectively, has been performed to discriminate the different carbon and hydrogen sources and the participation of the catalyst in the pathways involved in the whole cyclic process of the integrated capture of CO_2 and the regeneration with CH_4. The dual functionality of the catalyst showed a high chemical retention capacity of CO_2 (around 0.15 mmol $CO_2 \cdot g_{cat}^{-1}$) in basic Ni-Ba intermetallic centers together with the regeneration capacity through the injection of methane yielding to H_2-containing stream production. During the storage stage, the CO_2 adsorption and dissociative decomposition are the main reactions together with Boudouard reaction, whereas in the regeneration step, syngas was formed via chemical CO_2 reduction by CH_4, besides dry methane reforming.

1. Introduction

Carbon dioxide concentration in the atmosphere has been constantly increasing as a consequence of human activities and is considerably contributing to climate change, as the main component of greenhouse gases (GHG), followed by methane. Besides, CO_2 emissions represent the 81 % of total GHG with the transport and the electricity generation sectors currently making the greatest contribution, with almost 60 % of total emissions [1]. Despite the current climate action headed by the nations and the goals stated in the Paris Agreement, the level of atmospheric CO_2 continues rising at an alarming rate. The International Energy Agency, in World Energy Outlook 2019 Report, predicted a growth in the energy demand of 1.3 % per year until 2040 if the actual energy policies do not change (Current Policies Scenario). Although, the 2020 report proposed a slight decrease derived from the Covid-19 crisis depending on the duration of the pandemic and its economic and social impact, which caused an annual drop of 5 % in world energy demand [2–4], 2021 report estimated a rebound by 1.2 % (400 $MtCO_2$) below 2019 emissions levels because this increase of consumption. The electricity consumption is expected to increase at a higher rate respect to the demand of energy supply, driven by the utilization of industrial and vehicle electric engines and residential use. Even renewables have been accelerated (8 % between 2020 and 2021) which are destined to become the largest source of electricity generation in the world by 2025 and met 45 % of global electricity demand growth, coal and gas-fired power generation also increased approximately 4.5 % [4]. Regardless of the decrease of energy demand derived from Covid-crisis, the increase of renewable energies versus oil and coal was clear. All efforts are focused on the reduction of CO_2 from energy consumption. In this sense, different strategies have been considered to decrease the emissions from current gas and coal power plants, including Carbon Capture, Utilization and Storage (CCUS), or biomass co-fired devices; to repurpose them to focus on providing system adequacy and flexibility while reducing operations; or to retire them early.

Carbon Capture and Storage (CCS) is the most mature technology for CO_2 depletion. CO_2 capture at high temperature (greater than 500 °C) results attractive for industrial applications, due to the possibility of direct operation with the combustion gases, avoiding additional cooling steps. Main drawbacks for this technology are the regeneration of these types of compounds since decarbonation reaction yield CO_2-enriched

* Corresponding author.
E-mail address: luijo@uma.es (L.J. Alemany).

https://doi.org/10.1016/j.fuel.2023.127690
Received 26 May 2022; Received in revised form 30 December 2022; Accepted 3 February 2023
Available online 11 February 2023
0016-2361/© 2023 The Authors. Published by Elsevier Ltd. This is an open access article under the CC BY-NC-ND license (http://creativecommons.org/licenses/by-nc-nd/4.0/).

gas streams [5–9].

To face some of these limitations, a new technology based on Dual Function Materials was proposed, where a single material can capture the CO_2 and regenerate through a type of chemical loop, allowing the reduction of operation, transport, and storage costs, as the CO_2 is converted in situ into molecules of interest. Farrauto's group introduced this concept by reporting a Ru-based methanation catalyst and nano dispersed CaO as CO_2 adsorbent, both supported on a porous γ-Al_2O_3 carrier [10]. In this sense, the strategy of CO_2 revalorization into syngas using CH_4, as the second mist harmful gas in the atmosphere, via dry reforming (DRM) could be another alternative for the simultaneous reduction of two GHG emission.

Nickel has been recurrently used for CO_2 conversion [11,12], several factors have determined its wide application: its high activity, its abundancy and its relative low cost, compared to other metals. Tian et al. [13] used Ni in a calcium-looping methane reforming process using a CaO-Ni bifunctional sorbent-catalyst. First, CO_2 is captured by reacting with CaO adsorbent to form $CaCO_3$, then this is decomposed to bring CO_2 to the CaO-Ni interface for the reaction with CH_4 (dry reforming) to produce syngas according to the following equation:

$$CO_2(g) + CH_4(g) \leftrightharpoons 2CO\ (g) + 2H_2(g);\ \Delta H°r = +247.0\ kJ{\cdot}mol^{-1} \quad (1)$$

Furthermore, similar systems for cyclic CO_2-storage/conversion have been reported in the literature, including CO_2 storage and hydrogenation to CH_4 [14–17] and tri-reforming of methane for syngas production [18–20].

However, the major challenge for the CaO-based sorbents and the Ni-based catalysts is the fast decay of CO_2 capture performance and the deactivation of catalytic performance with the number of cycles, respectively [21]. Other investigations reported an improved activity by the incorporation of other components to the catalytic formulation, such as CeO_2 or Ru. The introduction of CeO_2 acting as a support to improve the catalytic activity has been studied extensively for the development of Ni-based catalysts [22]. Ruthenium has unique redox properties that allow it to rapidly reduce to its catalytically active state after exposure to an oxidizing environment (such as power plant flue gas) during the CO_2 capture step [14].

The development of advanced materials able to efficiently capture CO_2 and convert it into valuable chemicals (using a cyclic alternated technology based in LNT-NO_x catalytic system) represents a very interesting challenge.

Recently, Molina-Ramírez et al. [23] proposed a new Catalytic Technology (CO_2-SR: CO_2 Storage and in situ Regeneration with CH_4) for CO_2 depletion and H_2 production based on the dual-function concept. In this case, an unsupported Ni-Ba bimetallic catalyst operates in an alternating cyclic isothermally regime with consecutive pulses of CO_2 (storage steps) and CH_4 (regeneration steps), producing H_2-enriched streams, with a wide range of application in the energy and industry sector. Therefore, through an isotopic study, this work aims to go deep insight into the reactions involved in the two-step storage and regeneration process. The utilization of labelled molecules: $^{13}CO_2$ and CD_4 instead of $^{12}CO_2$ and CH_4 would allow to discriminate the different carbon and hydrogen sources and the participation of the catalyst in the whole cyclic process of CO_2 storage and CH_4 regeneration.

2. Experimental

2.1. Catalyst synthesis

An unsupported Ni-Ba bimetallic catalyst was synthesized with a Ni/Ba atomic ratio = 1/1 by coprecipitation of $Ni(NO_3)_2{\cdot}6H_2O$ and Ba $(NO_3)_2$ precursors (*Panreac Applichem*). A 3 wt% of total mass of atoms of colloidal silica was added (referred to Ni and Ba atomic content in the precursor solution). LUDOX HS-40 colloidal silica was purchased from *Aldrich* Chemistry (40 wt% SiO_2 in H_2O, surface area 198–258 m^2/g), as a surface area promoting and nucleation agent. Then, the generated gel was washed, dried for 24 h at 80 °C, and calcined at 800 °C (5 °C.min^{-1}) in air for 4 h. XRD X-ray Powder Diffraction data obtained with an X'Pert Pro MPD diffractometer (PANanalytical) using a $CuK_{\alpha 1}$ radiation (λ = 1.5406 Å) and a Ge(1 1 1) primary monochromator are included. Further details of preparation and characterization were early reported by Molina-Ramírez et al. [23].

2.2. Catalytic test and isotopic experiments

Catalytic cyclic tests for CO_2 Storage and Regeneration with CH_4 were performed isothermally at atmospheric pressure, using Transient Response Method (TRM) in a "U-shaped" quartz fixed-bed reactor (d_i = 6 mm) with down-flow connected to a *QMS 200* mass spectrometer (*Pfeiffer Vacuum Prisma™*). In each experiment, 60 mg of NiBa catalyst were used, maintaining a total inlet flow gas of 50 mL·min^{-1} and a space velocity GHSV of 1 0.06·$10^4 h^{-1}$. Inlet gases were fed at reactor with flow mass controllers (*PID-flow controller*) attached to a motorized valve that allowed instantaneous feed changes in the supply. Prior to each experiment, the catalyst was reduced *ex situ* in 20 %H_2-He atmosphere for 2 h at 600 °C and was conditioned in situ in He up to 600 °C, and then activated in a He-balanced H_2 stream (2 %H_2-He, 50 mL·min^{-1}) for 1 h, followed by He purge until all signals reach baseline.

Three different experiment-set were performed as it is represented in Fig. 1: Type I runs, consisting of alternated cycles of CO_2-He-CH_4, Type II runs, consisting of alternated cycles with labelled-C, $^{13}CO_2$-He-CH_4 and Type III runs, consisting of alternated cycles with labelled H, CO_2-He-CD_4. More specifically, pulses of 5 min of each gas reagent (10,000 ppm of CO_2 for storage step and CH_4 for regeneration one diluted in He) were alternated with a He-purge of 15 min; this allowed the stabilization of all m·z^{-1} signals after the previous pulse using Argon as a tracer.

The same experimental set was performed at 600, 650 and 700 °C, in order to evaluate the temperature effect. Outlet gases were analyzed with a mass spectrometer and the studied m·z^{-1} signals were: 2 (H_2), 3 (D_2), 4 (He), 12 (C), 13 (^{13}C), 14 (N), 16 (CH_4), 17 (H_2O), 19 (D_2O), 20 (CD_4), 28 (CO), 29 (^{13}CO), 32 (O_2), 40 (Ar), 44 (CO_2) and 45 ($^{13}CO_2$). These signals were selected in order to avoid any influence between the species and were normalized and most of them are calibrated. In all cases Ar was used as a tracer. Before running each type of experiment, a test without catalyst was performed, and the recorded mass spectrometry (MS) lines were used as a blank. Moreover, all the signals were normalized respect to its maximum intensity during each experiment.

In previous works [23], it was demonstrated that during the storage step, CO_2 can be stored or converted whereas in the regeneration step CH_4 was only converted. For that, the equations and notation to describe the conversion of each reagent was different and it is indicated in Eqs. (2) – (5).

$$\%CO_2^{sto+conv} = \frac{F_{CO_2}^{stored+converted}}{F_{CO_2}^{in}}\cdot 100 = \frac{F_{CO_2}^{in} - F_{CO_2}^{out}}{F_{CO_2}^{in}}\cdot 100 \quad (2)$$

$$\%\ {}^{13}CO_2^{sto+conv} = \frac{F_{CO_2}^{stored+converted}}{F^{in}{}_{^{13}CO_2}}\cdot 100 = \frac{F^{in}{}_{^{13}CO_2} - F^{out}{}_{^{13}CO_2}}{F^{in}{}_{^{13}CO_2}}\cdot 100 \quad (3)$$

$$\%CH_4^{conv} = \frac{F_{CH_4}^{converted}}{F_{CH_4}^{in}}\cdot 100 = \frac{F_{CH_4}^{in} - F_{CH_4}^{out}}{F_{CH_4}^{in}}\cdot 100 \quad (4)$$

$$\%CD_4^{conv} = \frac{F_{CD_4}^{converted}}{F_{CD_4}^{in}}\cdot 100 = \frac{F_{CD_4}^{in} - F_{CD_4}^{out}}{F_{CD_4}^{in}}\cdot 100 \quad (5)$$

Where F represents the flow equivalent in terms of area obtained from the integration of MS responses of CO_2 or $^{13}CO_2$ and CH_4 or CD_4 registered during storage and regeneration steps, respectively, extended almost for 10 alternating cycles. Each value was calculated from the third operation cycle in each experiment.

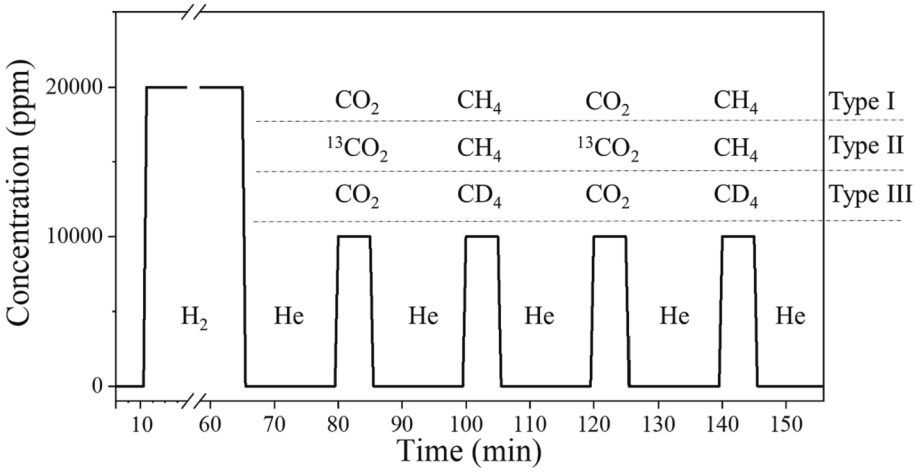

Fig. 1. Experimental set-up of the non-isotopic and isotopic runs performed to analyze the performance of NiBa catalyst in the CO_2-SR cyclic technology at any temperature. Reaction conditions: 50 mL·min^{-1}, GHSV of 1.06·10^{4}h^{-1}.

3. Results and discussion

It was stated that the NiBa catalyst is able to maintain its structure at high temperatures with a high reducibility even as bulk catalyst and presented well-balanced and distributed strong basic sites. XRD patterns and Raman spectra were previously published [23] for the NiBa catalyst calcined at 800 °C and reduced at 600 °C. For comparative purposes, in Fig. S1.a X-ray Diffractograms for the samples activated in hydrogen at 650 and 700 °C are represented and, however, Raman spectra of these samples are not included since there are no differences with the spectra obtained for the sample reduced at 600 °C. The disappearance of signals related to NiO and the identification of peaks associated with Ni^0 was confirmed at all the reduction temperatures. Crystallite size was calculated by Debye-Scherrer equation and the value was kept around 10 to 15 nm for all the samples reduced between 600 and 700 °C. A small amount of Ba can be found as $BaCO_3$ and Ba_2SiO_4 species that are not active in the process, whereas BaO was not observable by XRD and Raman. There is an effect of BaO on Ni particle species dispersion control because BaO interacts with Ni particles, since species where all the elements are well-distributed are observed (Fig S1.b). For the catalyst reduced at different temperature, the plausible formation of BaO-Ni nanointerphases exists, as was reported [23], where BaO interact with Ni species at surface level providing CO_2-chemi-adsorption sites that are even capable of carbon oxidation.

3.1. Type I runs for experiment validation

A set of experiments with non-labelled molecules was carried out as a catalytic test reference under isothermal transient regime using CO_2-He-CH_4 pulses (10,000 ppm feed gases as rectangular pulse). In Fig. 2 the CO_2 storage and regeneration mass spectrometer signal profiles for five CO_2-He-CH_4 consecutive cycles at 700 °C are shown.

Carbon monoxide and hydrogen signals along with the CO_2 fed were monitored and detected during CO_2 storage step, whereas CH_4, H_2, and CO were registered during the regeneration step (CH_4 pulse). The ion-current H_2O-signal appear to be perturbed during the whole

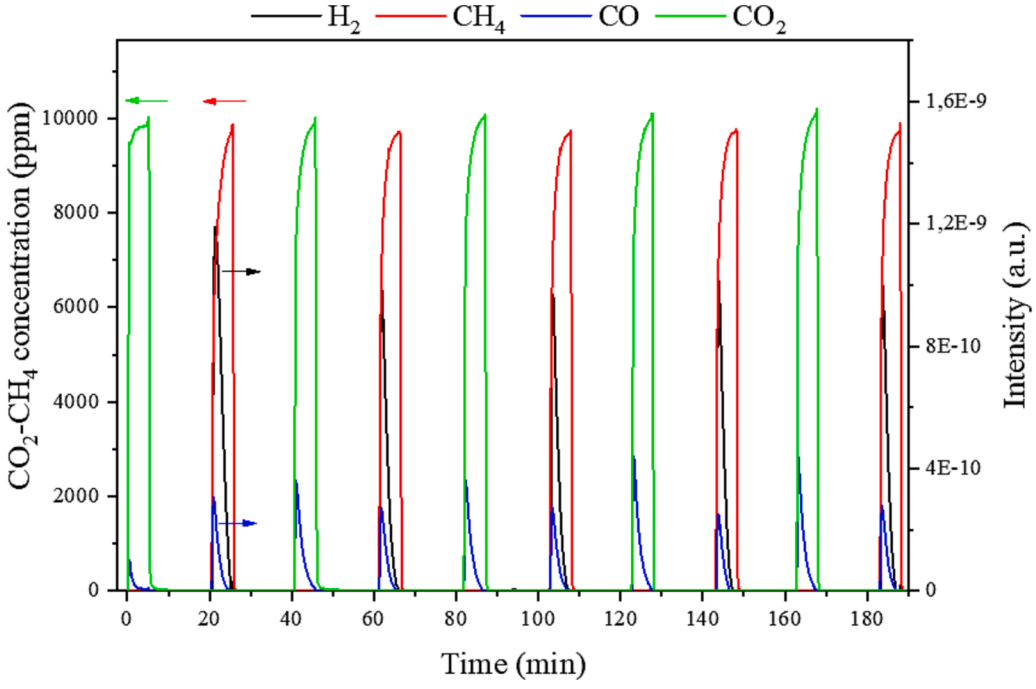

Fig. 2. H_2, CH_4, CO, CO_2 mass signals during CO_2-He-CH_4 alternating cycles (Type I runs) at 700 °C. Reaction conditions: 50 mL·min^{-1}, GHSV of 1.06·10^{4}h^{-1}.

experiment and unfortunately, the peak-shape was not well-defined inside of pulse-width and consequently was not included in the figures. It must be pointed out that the intensity of all the registered signals decreased during the He purge period, reaching values near zero, indicating a catalyst surface free of weakly-adsorbed molecules. The system reached a stable regime after three storage and regeneration cycles, near 80 min after the admission of CO_2 pulse, as the CO and H_2 signal profiles became comparable over the consecutive pulses until the end of the experiment.

To evaluate the performance, the outlet gas signal distribution registered during the storage and regeneration steps for the third cycle of Type I runs (CO_2-He-CH_4) at 700 °C was depicted in Fig. 3. Moreover, the profiles obtained at 600 and 650 °C can be found in supplementary information (Figure S2). During the storage-step, mass-signals corresponding to CO_2, CO, and H_2 were principally detected. The increase of the ($m{\cdot}z^{-1} = 44$) signal after the CO_2 injection is not instantaneous but progressive, yielding as the CO_2-breakthrough curve.

This CO_2 sigmoidal curve-shaped profile was related to the adsorption of CO_2 chemically bonded over the catalyst-surface resulting a useful storage capacity, whose values were estimated from the first cycle after H_2-reduction of catalyst and are shown in Table 1.

At 600 °C the CO_2 retention capacity was 0.6 % (0.126 $mmolCO_2{\cdot}g_{cat}^{-1}$) by weight of catalyst (adsorbed CO_2 mass/catalyst weight in percentage). The net CO_2 adsorption capacity continuously increased with temperature, reaching a maximum of 0.8 % (wt.) of CO_2 at 700 °C, the maximum tested temperature. The evolution of the CO_2 storage capacity depends on the temperature and a slight strengthening of the basic sites was proven. As was reported by A. Bermejo-Lopez et al. [24] using Al_2O_3 supported Ni-CaO catalyst a maximum CO_2 storage capacity around 520 °C was registered close to 0.17 $mmolCO_2{\cdot}g_{cat}^{-1}$, because the carbonated formed onto the alkaline-earth oxides present a high stability. The increase in temperature favors a deeper activation of the basic sites that promotes a higher CO_2 adsorption.

In the CO_2-step, mainly CO and H_2 signals were rapidly evolved. It is clearly noticeable that the hydrogen trace presented is due to the previous CH_4–step since it is absent in the first cycle. After that, the fed switched to He purge for 15 min. Subsequently, as regeneration-phase, CH_4 was injected into the system, and H_2, and CO were observed, together with the superimposed CH_4 signal, with a fast increased initially followed by a tail-end signal similar to that observed during the CO_2 storage phase. The intensity of the CH_4 signal progressively increases until saturation but, during this step, CH_4 was not stored but mainly reacts with the surface stored species to be converted to other molecules.

The calculated value $CO_2^{sto+conv}$ (i.e., stored and converted) during

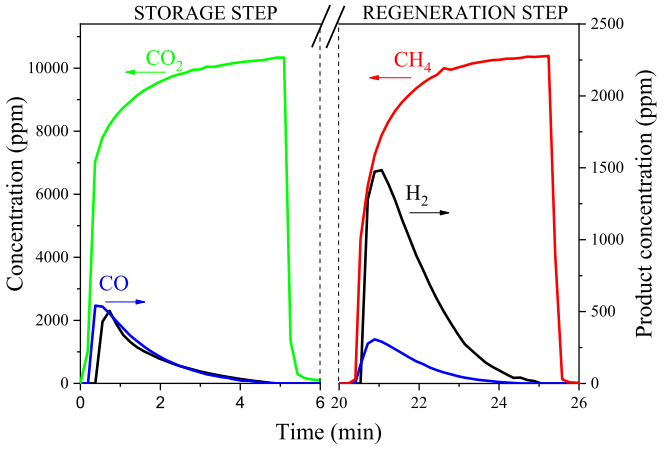

Fig. 3. Outlet gas signal distribution registered during the storage and regeneration steps for the third cycle of Type I runs (CO_2-He-CH_4) at 700 °C. Reaction conditions: 50 $mL{\cdot}min^{-1}$, GHSV of $1.06{\cdot}10^4 h^{-1}$.

Table 1
Adsorption capacity, conversion and selectivity ratio for Type I runs at different temperatures.

Temperature (°C)	Adsorption Capacity* (mmol $CO_2{\cdot}g_{cat}^{-1}$)	$CO_2^{sto+conv}$(%)**	CO/ H_2**	CH_4^{conv}(%)***	H_2/ CO***
600	0.126	8.18	2.35	14.52	25.45
650	0.142	8.51	1.48	19.14	8.17
700	0.183	9.21	1.21	20.19	5.31

*From the first cycle of CO_2-adsorption after reduction.
**From stable storage step.
*** From stable regeneration step.

the storage period was 9.2 % at 700 °C. For the regeneration period, CH_4^{conv} reached a value of 20.2 % and H_2/CO molar ratio of 5.3. These values are very far from the reported equilibrium conversion values at 700 °C for CO_2 and CH_4 (near 90 %, with CO_2 value slightly higher) when a $CO_2/CH_4 = 1$ ratio is co-fed, since in this work the reactants are fed separately under a discontinuous pulse feeding system (transitory regime). Besides, it should be considered that the material presented a relatively low CO_2 retention capacity and methane conversion was higher than CO_2 conversion values, due to side reactions that takes place during the regeneration step that increase methane conversion, such as methane decomposition as was reported in [23]. In our previous work [25], the results of dry catalytic reforming under transient experiment for a model Pt/Al_2O_3 type catalysts were reported and the CO_2 conversion values were systematically above the CH_4 conversion calculated values (47 and 36 % respectively). These differences could be in part due to the experimental procedure in which CH_4 and CO_2 are co-fed, and the type and functionality of catalysts which also activate CO_2 molecule instead of storing it.

The saturation curves for CO_2 and CH_4, in the storage and regeneration stages, respectively, have the same shape but the conversion estimated values of the reactants are different. For methane conversion, there is an increase with temperature, starting from 14.52 % at the lowest tested temperature, and the amount of CO_2 stored and converted also increase with temperature, varying from 8.18 to 9.21 %, as can be observed in Table 1. During the storage and regeneration periods both CO and H_2 appear. In the storage stage, as the CO/H_2 molar ratio is higher than 1, it suggests that the predominant reaction should be the formation of CO. During the regeneration stage, the H_2/CO molar ratio is higher than 1 and higher than the stoichiometric ratio of the reforming, indicating the occurrence of a hydrogen production process that is favoured by temperature. Although hydrogen production increases with temperature, H_2/CO ratio decreases from 25.5 to 5.3 because the amount of CO formed increases in a higher proportion, indicating a more pronounced effect of the temperature in the reactions that include CO production.

In a first approximation based on this type of experiments, the reactions that must be involved in the CO_2-SR technology are:

Storage stage

$$2CO_2(ads) \rightarrow CO_2^{sto} + CO(g) + O^* \quad (6)$$

$$CO_2(g) + C(s) \leftrightarrow 2CO(g) \quad (7)$$

$$C(s) + H_2O(ads) \leftrightarrow CO(g) + H_2(g) \quad (8)$$

Regeneration stage

$$CO_2^{sto} + CH_4(g) \rightarrow 2CO(g) + 2H_2(g) \quad (9)$$

$$CH_4(cat) \rightarrow CH_x(cat) \rightarrow C(s) + 2H_2(g) \quad (10)$$

3.2. Isotopic Type II and III experiments

The utilization of $^{13}CO_2$ and CD_4 as alternative carbon and hydrogen sources in Type II and III experiments, respectively, was an additional tool in order to understand the main reactions occurring in this CO_2-SR Cyclic Process over unsupported NiBa catalyst.

In Fig. 4, the product distribution during storage and regeneration phases corresponding to Type II experiment ($^{13}CO_2$-He-CH_4) at 650 °C is presented. Although no CO_2 neither CH_4 m·z^{-1} signals were represented, Ar does, so the start of each step of the cycle is indicated in the figure. The reagent and product profiles at all the tested temperatures can be found in Fig. S3. The Ni-BaO catalytic performance in terms of $CO_2^{sto+conv}$ and CH_4^{conv} values registered at 650 °C were 9.1 % and 16.4 %, respectively, similar to the data obtained in type I runs. In the storage stage, a CO sharp-signal formation is detected first and, with delay of several seconds, ^{13}CO is also detected. At all temperatures, the time-response and the ^{13}CO and CO profiles indicate the formation of these species preferentially during the storage step. In addition, a H_2-signal delay was also observed associated with H_2-chemisorbed release involving nickel sites or the gasification of carbon with hydroxylated centers. The instantaneous formation of unlabeled CO is related to the fact that gas $^{13}CO_2$ reacts directly with the deposited carbon (C(s)) species to give two molecules of labeled and unlabeled CO [Eq. (11)] [26]. Given that the calculated $^{13}CO/CO$ ratio is higher than 1, a parallel reaction associated with the dissociative decomposition reaction of the $^{13}CO_2$ fed occurs [Eq.12], at the basic sites of the catalyst, in agreement with the results obtained by other authors [27,28] working in a simultaneous feed of labeled CO_2 and CH_4. The release of the sites occupied by the adsorbed carbon allows the dissociative decomposition of the fed CO_2 and produces the delay in the maximum formation of labeled CO. Although the system is working in dry conditions C(s) could also react via gasification with hydroxylated surface (water from the regeneration step) [Eq.13], generating additional CO(g) and H_2(g) and this can explain the delayed hydrogen formation. Occasionally, the hydrogen formed could react with CO_2 through the reverse of Water Gas Shift [Eq.14], although the contribution of this reaction would be minor in this stage.

$$^{13}CO_2(g) + C(s) \leftrightarrow {}^{13}CO(g) + CO(g) \quad (11)$$

$$2\ {}^{13}CO_2(g) \rightarrow 2\ {}^{13}CO_2(ads) \rightarrow {}^{13}CO_2^{sto} + {}^{13}CO(g) + O^* \quad (12)$$

$$C(s) + H_2O(ads) \leftrightarrow CO(g) + H_2(g) \quad (13)$$

$$^{13}CO_2(g) + H_2(g) \rightarrow {}^{13}CO(g) + H_2O(g) \quad (14)$$

In the regeneration phase, by injecting a rectangular pulse of 10,000 ppm CH_4 after the $^{13}CO_2$ pulse, the formation of hydrogen was evidenced as a result of the catalytic methane decomposition with C(s) production, pointing out that methane activation in successive CH_x steps occurs over Ni-sites [Eq.15], as a well-known mechanism. In addition, the observing breakthrough signals of ^{13}CO and unlabeled CO in the regeneration phase suggests that the formation pathway, of these molecular species, come from methane reforming with $^{13}CO_2$ (ads) [Eqs. (16) and (17)]. For the conventional dry reforming reaction, the limiting step in the process is methane activation. However, on a surface partially enriched in CO_2 via carbonate formation, which occurs during the CO_2 storage stage, it cannot be ruled out that there is a fraction of CH_4 in the gas phase that can react with the CO_2 species stored on the catalyst surface, by chemical reduction and regeneration with the formation of syngas [Eq. (16)], in the named CO_2-storage and CH_4 regeneration reaction. Besides, the activation of both CO_2 and CH_4 occurs on the metal sites as a bifunctional mechanism, so CH_4 reacts directly from gas phase as commented above or via the activation on the metal surface giving CH_x (cat), forming syngas as conventional dry reforming mechanism [Eq. (17)]. It must be pointed out that due to the cyclic configuration used here, by the time CH_4(g) was injected, CO_2^{sto} was already adsorbed on the catalyst in form of carbonate species, avoiding the kinetic limitations associated with the CO_2 adsorption process. Since the CO-proportion content, $^{13}CO/CO$ ratio, is close to 0.20, the amount of CO detected at the outlet during the whole pulse is higher than the labelled molecule. This production comes from the oxidation of the CH_x species with the O* species from $^{13}CO_2$ decomposition [27] to form CO as consecutive reaction [Eq. (17)], and even this CO could also react with another dissociated O* to form newly CO_2 [Eq. (18)].

$$CH_4(cat) \rightarrow CH_x(cat) \rightarrow C(s) + 2H_2(g) \quad (15)$$

$$^{13}CO_2^{sto} + CH_4(g) \rightarrow {}^{13}CO(g) + CO(g) + 2H_2(g) \quad (16)$$

$$CH_x(cat) + O^* \rightarrow CO(g) + 2H_2(g) \quad (17)$$

$$CO(g) + O^* \rightarrow CO_2(g) \quad (18)$$

The influence of temperature in the reactions described above was evaluated, so, in Fig. 5, CO and ^{13}CO lines during storage and regeneration steps at 600, 650, 700 °C were showed. During the storage pulse, the maximum intensity of the sharp unlabeled CO signals increases appreciably with temperature, and the broad and asymmetric ^{13}CO signals are three times less intense than those of unlabeled CO, however, the trend is kept with the temperature increases. The $^{13}CO/CO$ ratio remains higher than 1, although this ratio depends on the temperature,

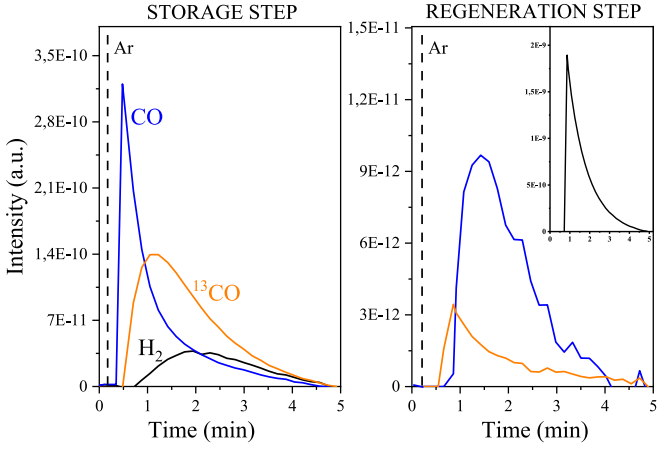

Fig. 4. Product distribution registered during the storage and regeneration steps for the third cycle of Type II runs ($^{13}CO_2$-He-CH_4) at 650 °C. Reaction conditions: 50 mL·min^{-1}, GHSV of 1.06·10^{4}h^{-1}.

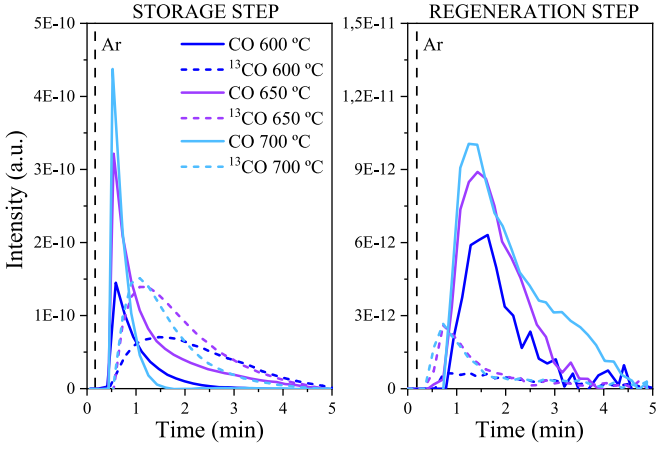

Fig. 5. CO and ^{13}CO mass signals during the storage and regeneration steps for the third cycle of Type II runs ($^{13}CO_2$-He-CH_4) at 600, 650, 700 °C. Reaction conditions: 50 mL·min^{-1}, GHSV of 1.06·10^{4}h^{-1}.

varying from 1.50 to 1.38 at increasing temperature. Quantitatively, and in terms of mmol of CO formed during the storage cycle, estimated from the area under the curve, the increase in the amount of ^{13}CO produced with temperature is confirmed, varying between 0.5, 0.7 and 1.1 μmol per cycle between 600, 650 and 700 °C, respectively. Similarly, the values recorded for unlabeled CO vary between 0.3 μmol at the lowest temperature tested and remain at approximate values of 0.6 μmol at temperatures greater than 650 °C. The linear trend in ^{13}CO production to increase with temperature is a direct consequence of dissociative adsorption and storage of $^{13}CO_2$ on the catalyst. On the other hand, the asymptotic trend around a value of 6 μmol of unlabelled CO indicates that the extent of the CO production reaction by gasification of the carbon formed on the catalyst surface [Eq. (11)] is limited by the amount of carbon deposited on the surface.

During regeneration, the amount of CO produced is an order of magnitude lower than that registered during the storage period, the $CO/^{13}CO$ ratio is higher than 1 and the intensity of both CO and ^{13}CO signals increased with temperature, evidencing the positive effect of temperature on endothermic reactions [29] and the higher methane conversion. A higher influence of temperature on the CO signal with respect to that of ^{13}CO has been observed, due to an increase of temperature favours the reaction [Eq. (17)] involving the activated methane (CH_x(cat)). The increase in the overall activity in this step is related to a higher population of active Ni-Ba species able to activate fed methane.

In order to study the reactions involved during the regeneration step and elucidate the hydrogen source during the storage step, methane was substituted by CD_4 in Type III runs. In Fig. 6, the product distribution registered during the storage and regeneration steps for the third cycle (CO_2-He-CD_4) at 600, 650 and 700 °C is represented. Additionally, in Supplementary Information (Fig. S4) the profiles of CO_2 and CD_4 together with CO and D_2 are also included at all tested temperatures. During the storage step, CO profiles were similar to those obtained in Type I experiments and the sum of CO and ^{13}CO in Type II runs. In addition, no significant changes are detected in the signals assigned to deuterium and H_2, indicating that the formation of hydrogen observed in type I and II experiments would be related to the intervention of surface OH species connected to Barium sites due to the water formed in the regeneration stage and represented as H_2O (ads) in Eq. (13). In the regeneration step, CO and D_2 were the detected products, being the former similar in shape to the profiles registered for experiments with unlabeled methane but slightly decreasing the overall production. On the other hand, a sharp D_2 signal was recorded with an intensity-one order of magnitude lower than that of hydrogen (compared in Fig. S5), which can be associated with a lower $m{\cdot}z^{-1}$ signal response at the same concentration or with the lower reduction capacity of the labeled methane. As can be observed, the production of all products increases with temperature in the same line that what has been previously detailed for Type I and II runs. Nevertheless, it is noteworthy that the conversion values of the reagents (CO_2 and CD_4) and the production of CO and D_2 were slightly lower than those of the experiments without labeled CH_4. These observations are in consonance with the effect registered by other authors when CH_4 is replaced by CD_4. A decrease in CD_4 conversion was detected in the methane oxidation [30] or in methane reforming with Ni-based catalysts [31–33], which can be related to a decrease in the CO formation rate and due to a low isotope effect.

According to these results, in the regeneration step, $CD_{4(g)}$ molecules react with the CO_2 retained during the previous storage step, generating $D_{2(g)}$ and $CO_{(g)}$ *via* Dry Reforming of isotopic Methane [Eq. (19)]. Moreover, the catalytic $CD_{4(cat)}$ decomposition [Eq. (20)] would provide more $D_{2(g)}$ and C(s), and the CD_x species necessary for the reaction with CO_2 in the dry reforming process [34] that react with the surface oxygen species to produce a higher amount of CO and D_2 [Eq. (21)].

$$CO_2^{sto} + CD_4(g) \rightarrow 2CO(g) + 2D_2(g) \quad (19)$$

$$CD_4(g) \rightarrow C(s) + 2D_2(g) \quad (20)$$

$$CD_x(cat) + O^* \rightarrow CO(g) + 2D_2(g) \quad (21)$$

Isotopic tracer study led us to corroborate a simple and rigorous mechanistic picture of the reaction network during alternating cycles and how Ni-clusters linked to BaO species on the catalyst surface favored the pathways of both CO_2 dissociation (activation) and CO formation by the reverse Boudouard reaction during the storage phase (caused by the interaction of dissociated CO_2 species and deposited carbon species) and the CH_4 decomposition process and catalytic reforming reactions involved along the regeneration phase, explaining the formation of the molecular species recorded. The percentage of CO_2-stored + converted and CH_4-conversion average values on Type I, II, and III runs are shown in Fig. 7, and were calculated from numerical integration of the $CO_2/^{13}CO_2$ or CH_4/CD_4 lines during storage and regeneration steps, respectively. Data were calculated from the third cycle, where a stable regime was reached. The conversion values at a given temperature were similar in all type runs, evidencing the reproducibility of the three types of experiments regardless of the kind of molecules injected. Nevertheless, the deviation in CH_4/CD_4 conversion values is around 4 % and higher than the values calculated for CO_2, which are lower than 1 %. This fact can be explained because of the kinetic isotope effect [35,36] that is referred to the effect on the reaction rate due to the isotopic

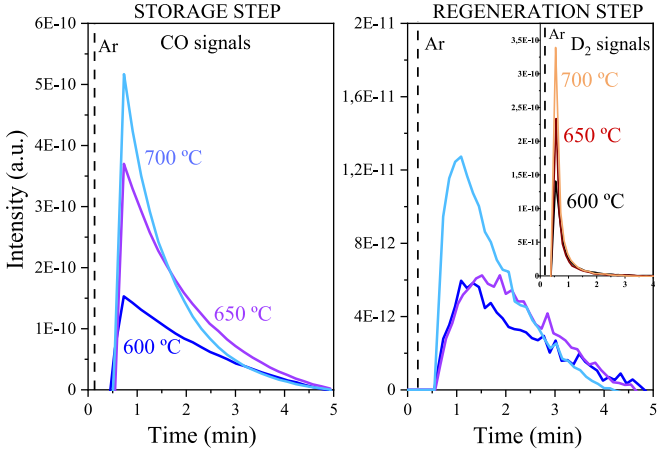

Fig. 6. Product distribution registered during the storage and regeneration steps for the third cycle of Type III runs (CO_2-He-CD_4) at 600, 650 and 700 °C. Reaction conditions: 50 $mL{\cdot}min^{-1}$, GHSV of $1.06{\cdot}10^4 h^{-1}$.

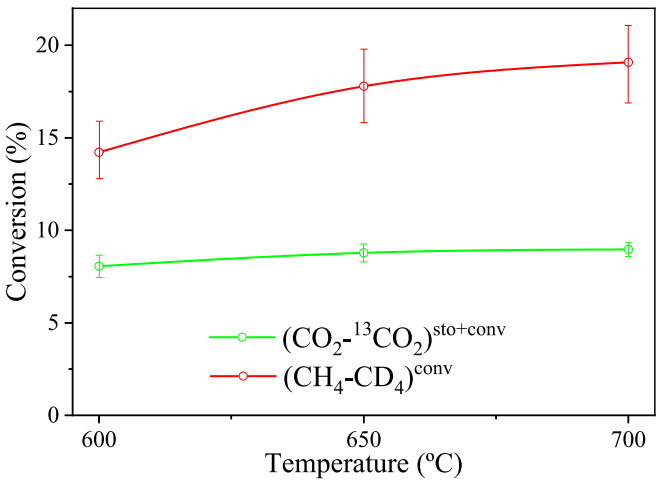

Fig. 7. Conversion mean values of the amount of CO_2 or $^{13}CO_2$ stored and converted and CH_4 or CD_4 converted values at 600, 650 and 700 °C. Reaction conditions: 50 $mL{\cdot}min^{-1}$, GHSV of $1.06{\cdot}10^4 h^{-1}$.

replacement of one or more bonds of the reactant. More specifically, when isotopic exchange refers to the replacement of hydrogen with deuterium, the properties of the bond are significantly affected. So, for the cleavage of a C-D bond, higher energy is required with respect to that for the C—H bond, producing the slight decrease in methane conversion.

3.3. Description of the CO_2-SR cyclic process

The study of the distribution of products in cyclic experiments and the use of isotopic molecules have allowed to establish the reactions involved in the CO_2-SR process. The NiBa unsupported catalyst has a dual function that requires centers capable of retaining CO_2 in the storage stage and other suitable sites that perform catalyst regeneration. In addition, the developed and potentially upgradeable Ni-Ba unsupported catalyst has shown a suitable performance. The presence of an alkaline-earth element in form of barium oxide is linked to the adsorption role during the storage stage due to the basic-site distribution. The presence of Ni metallic species ensures methane activation for the catalyst regeneration via chemical reduction. An interaction (Ni.BaO) has to exist that prevent sintering and limit the formation of spectator or catalytically inactive species. Furthermore, BaO increases the electron cloud density of Ni and the performance at a high reaction temperature range is also attributed to the highest amount of oxygen vacancies and Ni^0 stable centers on the catalyst surface as was reported previously [23].

Through the analysis of the product distribution obtained from isotopic and non-isotopic runs, a reaction process scheme was proposed and represented in Fig. 8. CO_2-SR technology utilizes a Ni-Ba unsupported catalyst, feeding CO_2, which is contained in the composition of a combustion gas-off, and methane, as one of two main components of biogas, during the storage and regeneration steps, respectively. During the storage step fed CO_2 is stored as labile carbonates on strong Ba-basic sites (identified as CO_2^{sto}) and the CO_2 dissociative decomposition also occurs in Ni interacting with BaO centers that are responsible of the formation of CO and O* species and is represented as a single reaction [Eq. (12)]. Furthermore, CO_2 reacts with the carbon deposited during the regeneration step by the reverse Boudouard reaction with CO formation [Eq. (11)], which was confirmed with the product distribution of the experiments with unlabeled and labeled CO_2. During the regeneration step, methane fed reacts with the CO_2 retained over the catalyst on Ni.BaO mixed reduced centers producing H_2 and CO as a bifunctional mechanism of dry reforming of methane indicated in Eqs. (16) and (17). Other reaction that increased CH_4 conversion values above CO_2 conversion values was methane decomposition with carbon and hydrogen formation [Eq. (15)]. The generated H_2(g) in this stage would promote the reduction of Ni-oxidized catalyst centers, thus regenerating the catalyst and producing water.

The analysis of the results with the isotopic study have led to a scheme that represents the reactions involved in the storage and regeneration stages in the CO_2-SR technology over NiO.BaO catalyst. It is possible to reach a high CO_2 conversion and the CH_4 catalyst regeneration yielding an enriched syngas stream. A potential syngas production technology based on CO_2 and methane was addressed by the availability of bio-based gas and the demand of technologies for potential utilization of carbon dioxide. The system presented here has a distinctive feature, as a proposal that revalorize methane, the second most harmful fluent gas for the atmosphere, to produce H_2, as a very efficient energetic vector whose combustion is carbon-free.

4. Conclusion

The study in transient regime with labeled molecules has allowed to delve into this novel catalytic technology of the integrated capture of CO_2 and the reaction of CH_4 as alternated pulses cyclic process in a fixed bed reactor configuration using an innovative NiBa unsupported catalyst. The catalyst has a dual functionality, showing a high chemical retention capacity of CO_2, with values of 0.8 wt% at 700 °C, comparable to other Dual Material Function-type systems. The regeneration capacity through the injection of methane yielding to H_2-containing stream production, with H_2/CO molar ratio between 5 and 25 in the analyzed temperature range. Isotopic tracer study, using $^{13}CO_2$ and CD_4, validated a mechanistic picture of the reactions network that occur during storage and regeneration alternated cycles and the tentative role of Ni and BaO species on the catalyst surface.

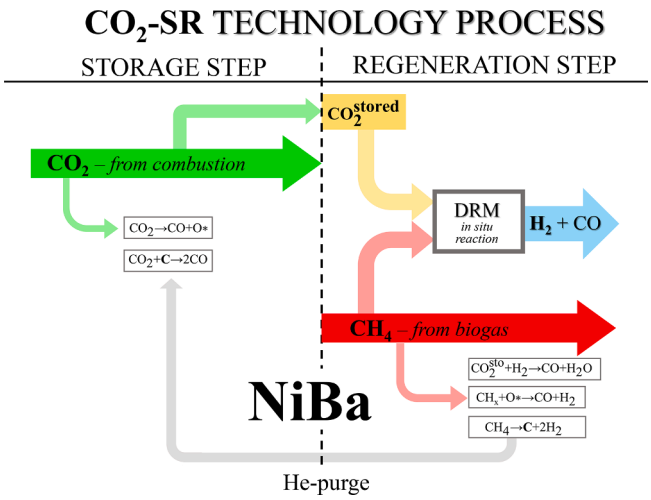

Fig. 8. Scheme of the process of cyclic alternated steps of the CO_2 (from combustion) storage and regeneration with CH_4 (from biogas) including the most remarkable reactions involved in CO_2-SR technology.

The individualization of stages and the product distribution, with labeled and unlabeled components through three series of experiments, allowed to stablish the main reactions involved in the CO_2-SR process. During the CO_2-storage stage, conversion and storage values around 8 % were estimated and ^{13}CO and CO profiles reveal the occurrence of the Boudouard reaction and the consecutive CO_2 adsorption and dissociative decomposition. In the regeneration stage, methane conversion values between 14 and 20 % were obtained in the range of 600–700 °C, with syngas formation via dry reforming and chemical reduction, and the additional methane decomposition causes an increase in the H_2/CO molar ratio, significantly higher than the stoichiometric value.

CRediT authorship contribution statement

S. Molina-Ramírez: Methodology, Investigation, Visualization, Writing – original draft. **D. Peltzer:** Methodology, Investigation, Visualization, Writing – original draft. **M. Cortés-Reyes:** Conceptualization, Investigation, Validation, Formal analysis, Writing – review & editing. **C. Herrera:** Conceptualization, Investigation, Validation, Writing – review & editing. **M.A. Larrubia:** Conceptualization, Investigation, Validation, Writing – review & editing. **L. Cornaglia:** Investigation, Visualization. **L.J. Alemany:** Conceptualization, Supervision, Writing – review & editing.

Declaration of Competing Interest

The authors declare that they have no known competing financial interests or personal relationships that could have appeared to influence the work reported in this paper.

Data availability

Data will be made available on request.

Acknowledgments

Funding for open access charge: Universidad de Málaga / CBUA.

Appendix A. Supplementary data

Supplementary data to this article can be found online at https://doi.org/10.1016/j.fuel.2023.127690.

References

[1] Energy Information Administration US. March 2022 Monthly Energy Review. 2022. https://www.eia.gov/totalenergy/data/monthly/pdf/mer.pdf.
[2] International Energy Agency (IEA). Global Energy Review 2019. OECD; 2020. 10.1787/90c8c125-en.
[3] International Energy Agency (IEA). Global Energy Review 2020. OECD; 2020. 10.1787/a60abbf2-en.
[4] International Energy Agency (IEA). World Energy Outlook 2021. OECD; 2021. 10.1787/14fcb638-en.
[5] Zhang Y, Gao Y, Pfeiffer H, Louis B, Sun L, O'Hare D, et al. Recent advances in lithium containing ceramic based sorbents for high-temperature CO_2 capture. J Mater Chem A 2019;7:7962–8005. https://doi.org/10.1039/c8ta08932a.
[6] Peltzer D, Múnera J, Cornaglia L. The effect of the Li: Na molar ratio on the structural and sorption properties of mixed zirconates for C_O2 capture at high temperature. J Environ Chem Eng 2019;7:102927. https://doi.org/10.1016/j.jece.2019.102927.
[7] Peltzer D, Mùnera J, Cornaglia L, Strumendo M. Characterization of potassium doped Li_2ZrO_3 based CO_2 sorbents: Stability properties and CO2 desorption kinetics. Chem Eng J 2018;336:1–11. https://doi.org/10.1016/j.cej.2017.10.177.
[8] Peltzer D, Salazar Hoyos LA, Faroldi B, Múnera J, Cornaglia L. Comparative study of lithium-based CO_2 sorbents at high temperature: Experimental and modeling kinetic analysis of the carbonation reaction. J Environ Chem Eng 2020;8:104173. https://doi.org/10.1016/j.jece.2020.104173.
[9] Hoyos LS, Faroldi B, Cornaglia L. Reactivity of rice husk-derived lithium silicates followed by in situ Raman spectroscopy. J Alloys Compd 2019;778:699–711. https://doi.org/10.1016/j.jallcom.2018.11.036.
[10] Duyar MS, Arellano Treviño MA, Farrauto RJ. Dual function materials for CO_2 capture and conversion using renewable H_2. Appl Catal B Environ 2015;168–169:370–6. https://doi.org/10.1016/j.apcatb.2014.12.025.
[11] Omodolor IS, Otor HO, Andonegui JA, Allen BJ, Alba-Rubio AC. Dual-Function Materials for CO_2 Capture and Conversion: A Review. Ind Eng Chem Res 2020;59:17612–31. https://doi.org/10.1021/acs.iecr.0c02218.
[12] Cao P, Zhao H, Adegbite S, Yang B, Lester E, Wu T. Stabilized CO_2 reforming of CH_4 on modified Ni/Al_2O_3 catalysts via in-situ K_2CO_3-enabled dynamic coke elimination reaction. Fuel 2021;298:120599. https://doi.org/10.1016/j.fuel.2021.120599.
[13] Tian S, Yan F, Zhang Z, Jiang J. Calcium-looping reforming of methane realizes in situ CO_2 utilization with improved energy efficiency. Sci Adv 2019:5. https://doi.org/10.1126/sciadv.aav5077.
[14] Arellano-Treviño MA, He Z, Libby MC, Farrauto RJ. Catalysts and adsorbents for CO_2 capture and conversion with dual function materials: Limitations of Ni-containing DFMs for flue gas applications. J CO_2 Util 2019;31:143–51. https://doi.org/10.1016/j.jcou.2019.03.009.
[15] Sun H, Wang J, Zhao J, Shen B, Shi J, Huang J, et al. Dual functional catalytic materials of Ni over Ce-modified CaO sorbents for integrated CO_2 capture and conversion. Appl Catal B Environ 2019;244:63–75. https://doi.org/10.1016/j.apcatb.2018.11.040.
[16] Sun H, Zhang Y, Guan S, Huang J, Wu C. Direct and highly selective conversion of captured CO_2 into methane through integrated carbon capture and utilization over dual functional materials. J CO_2 Util 2020;38:262–72. https://doi.org/10.1016/j.jcou.2020.02.001.
[17] Bermejo-López A, Pereda-Ayo B, González-Marcos JA, González-Velasco JR. Mechanism of the CO_2 storage and in situ hydrogenation to CH_4. Temperature and adsorbent loading effects over Ru-CaO/Al_2O_3 and Ru-Na_2CO_3/Al_2O_3 catalysts. Appl Catal B Environ 2019;256:117845. https://doi.org/10.1016/j.apcatb.2019.117845.
[18] Song C, Pan W. Tri-reforming of methane: a novel concept for catalytic production of industrially useful synthesis gas with desired H_2/CO ratios. Catal Today 2004;98:463–84. https://doi.org/10.1016/j.cattod.2004.09.054.
[19] Minutillo M, Perna A. A novel approach for treatment of CO_2 from fossil fired power plants, Part A: The integrated systems ITRPP. Int J Hydrogen Energy 2009;34:4014–20. https://doi.org/10.1016/j.ijhydene.2009.02.069.
[20] Kong F, Swift J, Zhang Q, Fan L-S, Tong A. Biogas to H_2 conversion with CO_2 capture using chemical looping technology: Process simulation and comparison to conventional reforming processes. Fuel 2020;279:118479. https://doi.org/10.1016/j.fuel.2020.118479.
[21] Sun H, Parlett CMA, Isaacs MA, Liu X, Adwek G, Wang J, et al. Development of Ca/KIT-6 adsorbents for high temperature CO_2 capture. Fuel 2019;235:1070–6. https://doi.org/10.1016/j.fuel.2018.07.044.
[22] Kambolis A, Matralis H, Trovarelli A, Papadopoulou C. Ni/CeO_2-ZrO_2 catalysts for the dry reforming of methane. Appl Catal A Gen 2010;377:16–26. https://doi.org/10.1016/j.apcata.2010.01.013.
[23] Molina-Ramírez S, Cortés-Reyes M, Herrera C, Larrubia MA, Alemany LJ. CO_2-SR Cyclic Technology: CO_2 Storage and in situ Regeneration with CH_4 over a new dual function NiBa unsupported catalyst. J CO_2 Util 2020;40:101201. https://doi.org/10.1016/j.jcou.2020.101201.
[24] Bermejo-López A, Pereda-Ayo B, González-Marcos JA, González-Velasco JR. Ni loading effects on dual function materials for capture and in-situ conversion of CO_2 to CH_4 using CaO or Na_2CO_3. J CO_2 Util 2019;34:576–87. https://doi.org/10.1016/j.jcou.2019.08.011.
[25] García-Diéguez M, Pieta IS, Herrera MC, Larrubia MA, Malpartida I, Alemany LJ. Transient study of the dry reforming of methane over Pt supported on different γ-Al_2O_3. Catal Today 2010;149:380–7. https://doi.org/10.1016/j.cattod.2009.07.099.
[26] Osaki T, Mori T. Kinetics of the reverse-Boudouard reaction over supported nickel catalysts. React Kinet Catal Lett 2006;89:333–9. https://doi.org/10.1007/s11144-006-0145-9.
[27] Kumar N, Kanitkar S, Wang Z, Haynes D, Shekhawat D, Spivey JJ. Dry reforming of methane with isotopic gas mixture over Ni-based pyrochlore catalyst. Int J Hydrogen Energy 2019;44:4167–76. https://doi.org/10.1016/j.ijhydene.2018.12.145.
[28] Bachiller-Baeza B, Mateos-Pedrero C, Soria MA, Guerrero-Ruiz A, Rodemerck U, Rodríguez-Ramos I. Transient studies of low-temperature dry reforming of methane over Ni-CaO/ZrO_2-La_2O_3. Appl Catal B Environ 2013;129:450–9. https://doi.org/10.1016/j.apcatb.2012.09.052.
[29] Merkouri LP, le Saché E, Pastor-Pérez L, Duyar MS, Ramirez RT. Versatile Ni-Ru catalysts for gas phase CO_2 conversion: Bringing closer dry reforming, reverse water gas shift and methanation to enable end-products flexibility. Fuel 2022;315:123097. https://doi.org/10.1016/j.fuel.2021.123097.
[30] Otsuka K, Wang Y, Sunada E, Yamanaka I. Direct partial oxidation of methane to synthesis gas by cerium oxide. J Catal 1998;175:152–60. https://doi.org/10.1006/jcat.1998.1985.
[31] Schuurman Y, Kroll VCH, Ferreira-Aparicio P, Mirodatos C. Use of transient kinetics techniques for studying the methane reforming by carbon dioxide. Catal Today 1997;38:129–35. https://doi.org/10.1016/S0920-5861(97)00046-1.
[32] Zhang Z, Verykios X. Performance of Ni/La_2O_3 catalyst in carbon dioxide reforming of methane to synthesis gas. Stud Surf Sci Catal 1997;107:511–6. https://doi.org/10.1016/s0167-2991(97)80383-7.
[33] Wang HY, Au CT. Carbon dioxide reforming of methane to syngas over SiO_2-supported rhodium catalysts. Appl Catal A Gen 1997;155:239–52. https://doi.org/10.1016/S0926-860X(96)00398-5.
[34] Cant NW, Dümpelmann R, Maitra AM. A comparison of nickel and rhodium catalysts for the reforming of methane by carbon dioxide. Stud Surf Sci Catal 1997;107:491–6. https://doi.org/10.1016/s0167-2991(97)80380-1.
[35] Gómez-Gallego M, Sierra MA. Kinetic Isotope Effects in the Study of Organometallic Reaction. Chem Rev 2011;111:4857–963. https://doi.org/10.1021/cr100436k.
[36] Kechagiopoulos PN, Angeli SD, Lemonidou AA. Low temperature steam reforming of methane: A combined isotopic and microkinetic study. Appl Catal B Environ 2017;205:238–53. https://doi.org/10.1016/j.apcatb.2016.12.033.